

The JCMT Nearby Galaxies Legacy Survey IV. Velocity Dispersions in the Molecular Interstellar Medium in Spiral Galaxies

C. D. Wilson¹, B. E. Warren^{1,2}, J. Irwin³, J. H. Knapen^{4,5}, F. P. Israel⁶, S. Serjeant⁷, D. Attewell¹, G. J. Bendo⁸, E. Brinks⁹, H. M. Butner¹⁰, D. L. Clements⁸, J. Leech¹¹, H. E. Matthews¹², S. Mühle¹³, A. M. J. Mortier¹⁴, T. J. Parkin¹, G. Petitpas¹⁵, B. K. Tan¹¹, R. P. J. Tilanus^{16,17}, A. Usero¹⁸, M. Vaccari¹⁹, P. van der Werf⁶, T. Wiegert²⁰, M. Zhu²¹

¹Department of Physics & Astronomy, McMaster University, Hamilton, Ontario L8S 4M1, Canada

²Currently at the International Centre for Radio Astronomy Research, University of Western Australia

³Department of Physics, Engineering Physics and Astronomy, Queen's University, Kingston, Ontario K7L 3N6, Canada

⁴Instituto de Astrofísica de Canarias, E-38200 La Laguna, Tenerife, Spain

⁵Departamento de Astrofísica, Universidad de La Laguna, E-38205 La Laguna, Tenerife, Spain

⁶Sterrewacht Leiden, Leiden University, PO Box 9513, 2300 RA Leiden, The Netherlands

⁷Department of Physics & Astronomy, The Open University, Milton Keynes MK7 6AA, United Kingdom

⁸Astrophysics Group, Imperial College, Blackett Laboratory, Prince Consort Road, London SW7 2AZ, United Kingdom

⁹Centre for Astrophysics Research, University of Hertfordshire, College Lane, Hatfield AL10 9AB, United Kingdom

¹⁰Department of Physics and Astronomy, James Madison University, MSC 4502 - 901 Carrier Drive, Harrisonburg, VA 22807, U.S.A.

¹¹Department of Physics, University of Oxford, Keble Road, Oxford OX1 3RH, United Kingdom

¹²National Research Council Canada, Herzberg Institute of Astrophysics, DRAO, P.O. Box 248, White Lake Road, Penticton, British Columbia V2A 69J, Canada

¹³Joint Institute for VLBI in Europe, Postbus 2, 7990 AA Dwingeloo, The Netherlands

¹⁴Scottish Universities Physics Alliance, Institute for Astronomy, University of Edinburgh, Royal Observatory, Blackford Hill, Edinburgh, EH9 3HJ, UK

¹⁵Harvard-Smithsonian Center for Astrophysics, 60 Garden St., MS-78, Cambridge, MA 02138, USA

¹⁶Joint Astronomy Centre, 660 N. A'ohoku Pl., University Park, Hilo, HI 96720, USA

¹⁷Netherlands Organisation for Scientific Research, Laan van Nieuw Oost-Indie 300, NL-2509 AC The Hague, The Netherlands

¹⁸Observatorio de Madrid, OAN, Alfonso XII, 3, E-28014 Madrid, Spain

¹⁹Dipartimento di Astronomia, Università di Padova, Vicolo dell'Osservatorio 5, 35122 Padua, Italy

²⁰Department of Physics and Astronomy, University of Manitoba, Winnipeg, Manitoba R3T 2N2, Canada

²¹National Astronomical Observatories, Chinese Academy of Sciences, 20A Datun Road, Chaoyang District, Beijing, China

11 June 2010

ABSTRACT

An analysis of large-area CO $J=3-2$ maps from the James Clerk Maxwell Telescope for 12 nearby spiral galaxies reveals low velocity dispersions in the molecular component of the interstellar medium. The three lowest luminosity galaxies show a relatively flat velocity dispersion as a function of radius while the remaining nine galaxies show a central peak with a radial fall-off within $0.2 - 0.4r_{25}$. Correcting for the average contribution due to the internal velocity dispersions of a population of giant molecular clouds, the average cloud-cloud velocity dispersion across the galactic disks is $6.1 \pm 1.0 \text{ km s}^{-1}$ (standard deviation 2.9 km s^{-1}), in reasonable agreement with previous measurements for the Galaxy and M33. The cloud-cloud velocity dispersion derived from the CO data is on average two times smaller than the HI velocity dispersion measured in the same galaxies. The low cloud-cloud velocity dispersion implies that the molecular gas is the critical component determining the stability of the galactic disk against gravitational collapse, especially in those regions of the disk which are H_2 dominated. The cloud-cloud velocity dispersion shows a significant positive correlation with both the far-infrared luminosity, which traces the star formation activity, and the K-band absolute magnitude, which traces the total stellar mass. For three galaxies in the Virgo cluster, smoothing the data to a resolution of 4.5 kpc (to match the typical resolution of high redshift CO observations) increases the measured velocity dispersion by roughly a factor of two, comparable to the dispersion measured recently in a normal

1 INTRODUCTION

The vertical structure of the interstellar medium is determined by a delicate balance between gravity and pressure. The concentration of mass in the stellar disk drags the gas into a thin disk whose vertical scale height is controlled by the velocity dispersion. The velocity dispersion of the gas is also an important parameter for star formation laws based on the Toomre Q criterion (Toomre 1964; Kennicutt 1989). The atomic phase of the interstellar medium (ISM) has been well studied and interpreted, most recently by Tamburro et al. (2009, see below). However, the velocity dispersion of the star forming molecular gas is much less well understood, although the available data are consistent with a significantly thinner and dynamically colder molecular disk (Stark & Brand 1989; Wilson & Scoville 1990; Combes & Becquaert 1997).

Determining the velocity dispersion of the molecular gas in the Galaxy is complicated by our location within the plane of the disk and the difficulty in removing the effects of streaming motions associated with spiral arms. Nearby, relatively face-on galaxies are better targets, provided sufficient sensitivity and spectral and spatial resolution can be achieved. However, an additional complicating factor in any analysis is the fact that the observed velocity dispersions are not significantly larger than the internal velocity dispersion of an individual giant molecular cloud (GMC). For example, Solomon et al. (1987) measure internal velocity dispersions ranging from 1 to 8 km s⁻¹ and a relation between internal velocity dispersion and cloud mass that goes as $M = 2000\sigma_v^4$. Certainly the net effect of the internal velocity dispersion of a population of giant molecular clouds in the beam needs to be considered in an analysis of the cloud-cloud velocity dispersion of nearby, near face-on galaxies.

For our own Galaxy, Clemens (1985) obtained a one-dimensional cloud-cloud velocity dispersion of 3.0 km s⁻¹, significantly smaller than the value of 7-9 km s⁻¹ obtained by Stark (1984). Stark & Brand (1989) argue that the velocity dispersion measured by Clemens (1985) is actually the internal velocity dispersion of individual clouds and obtain a cloud-cloud velocity dispersion of 7.8 ± 0.6 km s⁻¹ for clouds within 3 kpc of the Sun. Although this measurement includes small-scale streaming motions, they argue that the true value is only 20% smaller when the streaming motions are removed (Stark & Brand 1989). More recently Stark & Lee (2005, 2006) have re-derived the scale height of the molecular gas to be 35 pc for clouds less massive than $2 \times 10^5 M_\odot$ and only 20 pc for clouds more massive than this limit. This scale height of 20 pc implies a one-dimensional cloud-cloud velocity dispersion of just 4 km s⁻¹ for the more massive molecular clouds. Combes & Becquaert (1997) point out that, given the observed scale heights of HI and CO in the Galaxy and a velocity dispersion of 9 km s⁻¹ in the atomic gas, we would expect a cloud-cloud velocity dispersion of only 2.4 km s⁻¹ in the molecular gas, a value which is significantly smaller than any of the measurements.

There are relatively few measurements of the velocity dispersion of the molecular gas in other galaxies. Wilson & Scoville (1990) used a combination of interferometric observations of individual giant molecular clouds with single dish observations of M33 to measure a cloud-cloud velocity dispersion of 5 ± 1 km s⁻¹.

Combes & Becquaert (1997) observed NGC 628 and NGC 3938 using the CO $J=1-0$ and $J=2-1$ lines and observed velocity dispersions of 6 km s⁻¹ and 8.5 km s⁻¹, respectively. They used gaussian fits to the observed line widths and corrected for saturation effects (García-Burillo et al. 1993). Walsh et al. (2002) made CO $J=1-0$ and $J=3-2$ observations of NGC 6946 and measured velocity dispersions from second moment maps of 8.9 ± 2.2 km s⁻¹ and 6.0 ± 1.6 km s⁻¹ in the two lines. Neither of these two studies (Combes & Becquaert 1997; Walsh et al. 2002) attempted to correct for the internal velocity dispersion of individual GMCs, and so these measurements are upper limits to the cloud-cloud velocity dispersion.

There have been a number of theoretical attempts to model the cloud-cloud velocity dispersion in the Galaxy. Jog & Ostriker (1988) propose that cloud-cloud gravitational scattering in a differentially rotating galactic disk acts to increase the random kinetic energy of the cloud population. In this model, inelastic collisions between clouds act as an energy sink, resulting in an equilibrium value for the one-dimensional velocity dispersion of 5-7 km s⁻¹. Gammie, Ostriker & Jog (1991) extended this work using both analytical and numerical analyses and obtain a value of 5 km s⁻¹ for the two-dimensional velocity dispersion in the plane of the disk. Thomasson et al. (1991) performed N body simulations of clouds and stars which include inelastic cloud collisions but not close 2-body gravitational encounters. They find typical velocity dispersions of 3 km s⁻¹ which increase in galaxies with stronger spiral structure. More recently, Tasker & Tan (2009) have developed a three dimensional model including ISM cooling to 300 K with a resolution of 8 pc and find typical velocity dispersions of 10 km s⁻¹ for a model of the Milky Way.

Although there have been relatively few measurements of the velocity dispersion in the molecular gas in galaxies, the velocity dispersion of the atomic gas has been well studied (see Tamburro et al. 2009, and references therein). Most recently, the THINGS survey (Walter et al. 2008) has produced high-resolution HI maps of 34 spiral and irregular galaxies with distances less than 11 Mpc. The typical velocity dispersion in the atomic gas at radii between $r_{25}/2$ and r_{25} is 11 ± 3 km s⁻¹ for galaxies with inclinations less than 60° (Leroy et al. 2008). Tamburro et al. (2009) find an HI line width that falls off systematically with radius which they link to the energy provided by supernovae linked to recent star formation. They also find a characteristic HI velocity dispersion of 10 ± 2 km s⁻¹ at r_{25} , which often marks the extent of significant star formation in the disk.

In this paper, we present measurements of the velocity dispersion for the molecular component of the interstellar medium using data from the JCMT Nearby Galaxies Legacy Survey (NGLS) as well as a follow-up program on HI-rich spiral galaxies in the Virgo Cluster. We use new, wide-area observations of the CO $J=3-2$ emission for 12 large spiral galaxies with inclinations < 60° and distances < 17 Mpc. We discuss the observations, data reduction, and analysis methods used in §2. A more detailed comparison with the results of Combes & Becquaert (1997) is given in Appendix A. In §3, we discuss the observed values of the velocity dispersion of the CO $J=3-2$ transition and the correction factor necessary due to the non-trivial internal velocity dispersion of individual giant molecular clouds. The potential need to cor-

rect for a non-isotropic velocity dispersion in galaxies with inclinations larger than about 30° is discussed in Appendix B. In §4, we compare our results with recent observations of the velocity dispersion of the atomic gas component from the THINGS survey (Walter et al. 2008), investigate correlations of the velocity dispersion of the molecular gas with global galaxy properties such as mass and star formation rate, discuss the implications for understanding disk stability in galaxies, and compare our data with recent observations of spiral galaxies at $z = 1$. We give our conclusions in §5.

2 OBSERVATIONS AND DATA PROCESSING

2.1 JCMT CO $J=3-2$ data

The CO $J=3-2$ observations were obtained as part of the JCMT Nearby Galaxies Legacy Survey (NGLS)^a, which is observing an HI flux limited sample of 155 galaxies within 25 Mpc (Wilson et al. 2009). The angular resolution of the JCMT at this frequency is $14.5''$, which corresponds to a linear resolution ranging from 0.2 to 1.2 kpc for the galaxies in our sample. From the large ($D_{25} > 4'$) spiral galaxies observed by the NGLS, we selected 9 galaxies with inclinations smaller than 60° to study the velocity dispersion. Eight additional large galaxies from the NGLS with low inclinations (IC 2574, UGC 04305, NGC 3031, NGC 3351, NGC 4450, NGC 4579, and NGC 4725) did not have sufficiently strong or extended detections in CO $J=3-2$ to be useful for this analysis. To this sample we added three spiral galaxies in the Virgo Cluster (NGC 4303, NGC 4501, and NGC 4535) which are not part of the NGLS survey but which have been observed in a similar manner. (A fourth Virgo Cluster galaxy, NGC 4548, did not have a strong enough detection to be useful here.) These galaxies were observed as part of a follow-up program to the NGLS (JCMT proposal M09AC05, PI C. Wilson) to obtain CO $J=3-2$ observations to complete the sample of Virgo spiral galaxies with HI fluxes > 6.3 Jy km s^{-1} . The data for these three galaxies were obtained between 2009 February 14 and 2009 May 26.

Relevant properties of the 12 galaxies are given in Table 1. All 12 galaxies were observed in raster mapping mode to cover a rectangular area corresponding to $D_{25}/2$ with a 1 sigma sensitivity of better than 19 mK (T_A^*) at a spectral resolution of 20 km s^{-1} . We used the 16 pixel array receiver HARP-B (Buckle et al. 2009) with the ACSIS correlator configured to have a bandwidth of 1 GHz and a resolution of 0.488 MHz (0.43 km s^{-1} at the frequency of the CO $J=3-2$ transition). The combination of uniquely high velocity resolution and large mapping area is critical for accurate measurements of the velocity dispersion in the molecular interstellar medium.

Details of the reduction of the CO $J=3-2$ data are given in Wilson et al. (2009) and Warren et al. (2010) and so we discuss here only the most important processing steps and those steps that differed from the previous analysis. The individual raw data files were flagged to remove data from any of the 16 individual receptors with bad baselines and then the scans were combined into a data cube using a

$\text{sinc}(\pi x)\text{sinc}(k\pi x)$ kernel as the weighting function to determine the contribution of individual receptors to each pixel in the final map. The pixel size in the maps is $7.276''$. A mask was created to identify line-free regions of the data cube and a first-order baseline was fit to those line-free regions and subtracted from the cube.

We then used the clumpfind algorithm (Williams et al. 1994) implemented as part of the CUPID^b (Berry et al. 2007) task findclumps to identify regions with emission with signal-to-noise greater than 2.5 in a data cube that had been boxcar smoothed by 3x3 spatial pixels and 25 velocity channels. Moment maps were created from the original data cube after applying the mask created by findclumps. The moment maps which are the focus of this paper are the moment 2 maps, which measure the velocity dispersion, σ_v , for each pixel in the image using

$$\sigma_v = \sqrt{\Sigma T_i (v_i - \bar{v})^2 / \Sigma T_i}$$

where v_i and T_i are the velocity and temperature of a given velocity channel and \bar{v} is the intensity weighted mean velocity of that pixel. This method of calculating the velocity dispersion differs from that used by Combes & Bica (1997), who fit gaussian profiles to the CO lines. However, in the limit of gaussian lines with a high signal-to-noise ratio, the values from the moment 2 maps should agree with the results from fitting a gaussian directly to the line profiles. A more detailed comparison of our data with Combes & Bica (1997) is given in Appendix A. Moment 2 maps are often used to determine the velocity dispersion in the atomic gas, although this method is most reliable for simple line shapes, as warped disks and HI at large scale heights can distort the line profiles (de Blok et al. 2008).

Because we were using a relatively low signal-to-noise threshold in creating our masks, the final moment 2 maps sometimes appeared to contain spuriously high values typically in the outer portions of the map. These regions appear white in Figures 1 and 2. These values would bias the dispersions upward if they were included in our averages. For 5 galaxies in our sample, (NGC 4321, NGC 628, NGC 2403, NGC 3184, and NGC 4826), we applied an upper threshold to remove pixels with values that were higher than the highest value seen in the central part of the galaxy. The thresholding values used were 15 km s^{-1} for NGC 628, 25 km s^{-1} for NGC 2403 and NGC 3184, 52 km s^{-1} for NGC 4321, and 85 km s^{-1} for NGC 4826. We also applied a threshold cut of 65 km s^{-1} to NGC 4501 but very high values persisted in the north-western portion of the map (see below); the velocity dispersions in Table 1 are measured in the south-east portion of the map only. For NGC 5055, we used a targeted threshold to remove the block of high values seen in the north-east portion of the map.

2.2 HI data from THINGS

For the 6 galaxies (NGC 628, NGC 2403, NGC 3184, NGC 4736, NGC 4826, and NGC 5055) that are in common be-

^b CUPID is part of the Starlink (Currie et al. 2008) software package, which is available for download from <http://starlink.jach.hawaii.edu>

^a <http://www.jach.hawaii.edu/JCMT/surveys/>

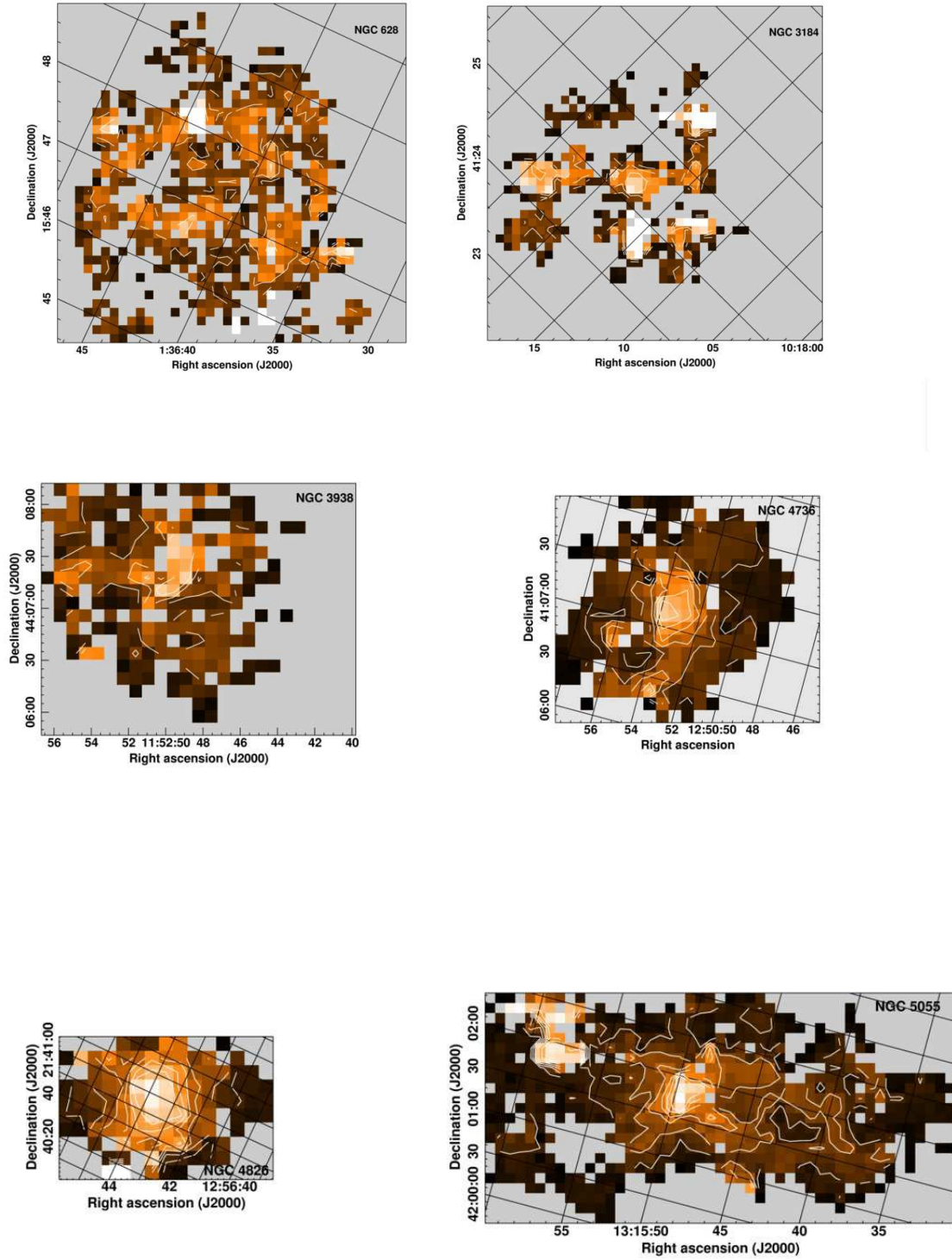


Figure 1. CO $J=3-2$ velocity dispersion for six galaxies which are not members of the Virgo cluster. (a) NGC 628. Contour levels are 2.5, 5, 10 km s^{-1} and the colour scale peak is 15 km s^{-1} . (b) NGC 3184. Contour levels are 5, 10, 15 km s^{-1} and the colour scale peak is 25 km s^{-1} . (c) NGC 3938. Contour levels and colour scale are the same as for NGC 3184. (d) NGC 4736. Contour levels are 10, 20, ... 60 km s^{-1} and the colour scale peak is 85 km s^{-1} . (e) NGC 4826. Contour levels and colour scale are the same as for NGC 4736. (f) NGC 5055. Contour levels and colour scale are the same as for NGC 4736.

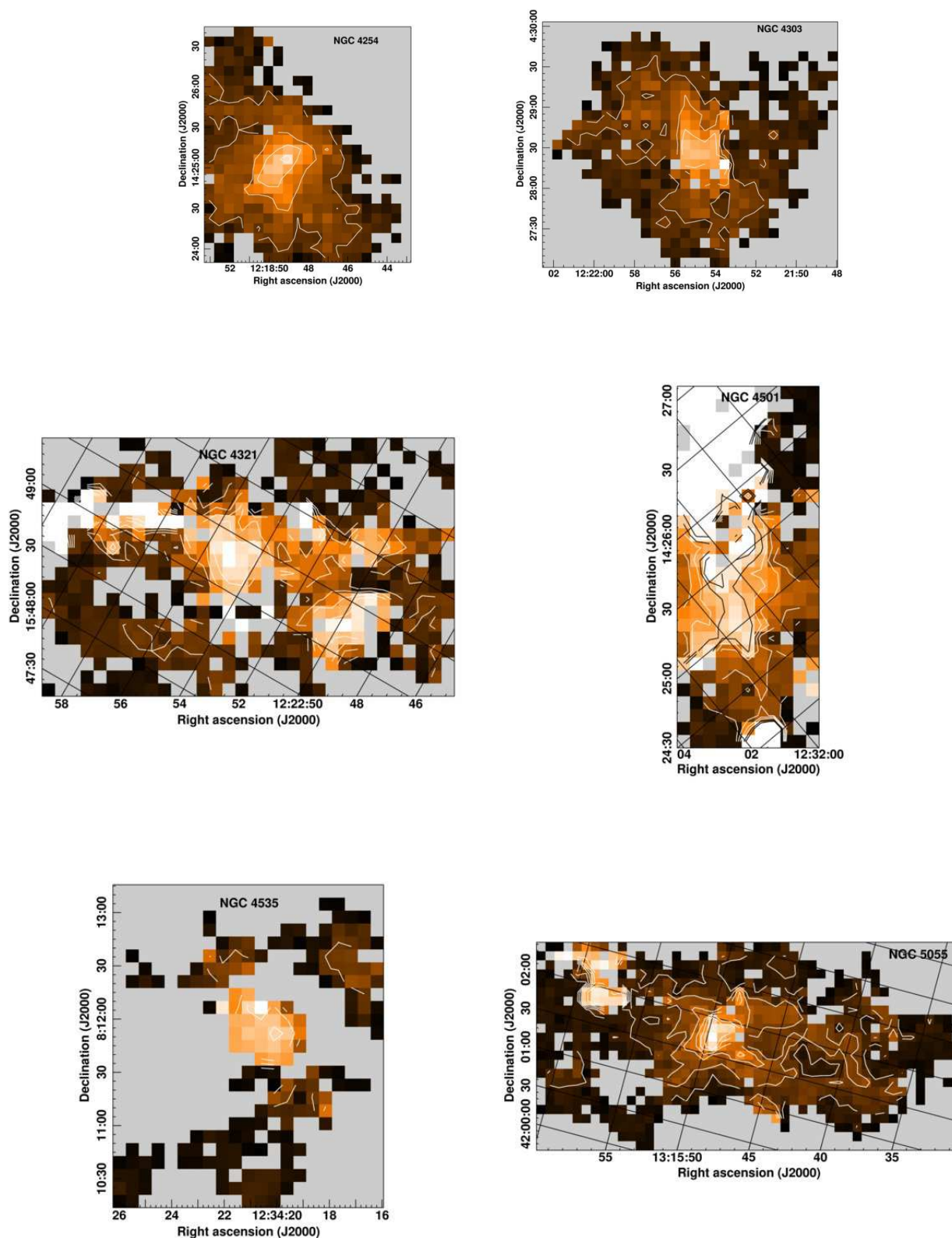


Figure 2. CO $J=3-2$ velocity dispersion for five galaxies which are members of the Virgo cluster and NGC 2403, which is the closest galaxy in our sample. Colour scale runs from 0 (black) to 50 km s^{-1} (white) and contour levels are 10, 20, 30, 40, 50 km s^{-1} unless otherwise noted. (a) NGC 4254. (b) NGC 4303. (c) NGC 4321. (d) NGC 4501. Contour levels are 10, 20, ... 60 km s^{-1} and the colour scale peak is 65 km s^{-1} . (e) NGC 4535. (f) NGC 2403. Contour levels are 5, 10, 15 km s^{-1} and the colour scale peak is 25 km s^{-1} .

Table 1. Galaxy Properties and Velocity Dispersions

Galaxy	V_{hel} (km s ⁻¹)	Type ^a	D_{25}^a (')	i^a (°)	PA^b (°)	$K(tot)^c$ (mag)	$\log L_{FIR}^d$ (L _⊙)	Distance ^e (Mpc)	σ_{obs}^f (km s ⁻¹)	σ_{c-c}^g (km s ⁻¹)	σ_{HI}^h (km s ⁻¹)
NGC 628	648	SA(s)c	10.5	7	20	6.84	9.55	7.3	4.1 ± 2.5	3.5 ± 0.1	12
NGC 2403	121	SAB(s)cd	21.9	56	124	6.19	9.10	3.2	5.2 ± 4.9	3.9 ± 0.2	14
NGC 3184	574	SAB(rs)cd	7.4	16	179	7.78	9.69	11.1	6.8 ± 5.9	5.8 ± 0.4	13
NGC 3938	829	SA(s)c	5.4	25	52	7.81	9.72	14.2	4.4 ± 2.9	2.7 ± 0.3	10 ⁱ
NGC 4254	2412	Sa(s)c	5.4	29	56	6.93	10.62	16.7	9.2 ± 4.5	8.5 ± 0.3	...
NGC 4303	1577	SAB(rs)bc	6.5	17	318	6.84	10.59	16.7	8.0 ± 4.2	7.2 ± 0.2	...
NGC 4321	1599	SAB(s)bc	7.6	32	143	6.59	10.47	16.7	12 ± 11	11.1 ± 0.6	...
NGC 4501	2213	SA(rs)b	6.9	58	140	6.27	10.41	16.7	20 ± 15	20 ± 2	...
NGC 4535	1972	SAB(s)c	7.1	41	0	7.38	10.12	16.7	5.1 ± 4.4	3.7 ± 0.4	...
NGC 4736	295	(R)SA(r)ab	11.2	36	296	5.11	9.79	5.2	12 ± 9	11.9 ± 0.7	25
NGC 4826	390	(R)SA(rs)ab	10.0	57	121	5.33	9.85	7.5	14 ± 11	13 ± 2	60
NGC 5055	495	SA(rs)bc	12.6	59	102	5.61	10.30	8.0	9.4 ± 6.6	8.7 ± 0.3	24

^a Buta et al. (2007)^b Position angle used for radial averages. NGC 628, NGC 3184: Tamburro et al. (2008); NGC 2403, NGC 4736, NGC 4826, NGC 5055: de Blok et al. (2008); NGC 3938: Paturel et al. (2000); NGC 4254, NGC 4303, NGC 4501, NGC 4535: (Cayatte et al. 1990); NGC 4321: Knapen et al. (1993).^c K-band total apparent magnitude from Jarrett et al. (2003).^d From Sanders et al. (2003) adjusted for the distances adopted here.^e NGC 628: Karachentsev et al. (2004); NGC 2403: Freedman et al. (2001); NGC3184: Leonard et al. (2002); NGC 3938, NGC 5055: distance calculated using Hubble flow distance with velocity corrected for Virgo infall (Mould et al. 2000) and $H_o = 73 \text{ km s}^{-1} \text{ Mpc}^{-1}$; Virgo Cluster: Mei et al. (2007); NGC 4736, NGC 4826: Tonry et al. (2001).^f Observed CO $J=3-2$ velocity dispersion and standard deviation. Regions of high velocity dispersion in the outer portions of the disk were masked before calculating the velocity dispersion (see text). Excludes a 5.3 kpc diameter region in the centre of each Virgo galaxy (9 pixels), NGC 3938 (11 pixels) and NGC 5055 (19 pixels). All pixels are included for NGC 628, NGC2403, and NGC 3184. For NGC 4736 and NGC 4826, a 9 pixel region is excluded to give an upper limit to the outer disk velocity dispersion (see text). Note that the uncertainty in the mean for σ_{obs} is the same as for σ_{c-c} .^g Mean cloud-cloud velocity dispersion and the uncertainty in the mean corrected for the contribution from the internal velocity dispersion of individual giant molecular clouds (see text). Note that the uncertainty in the mean is calculated from the standard deviation given in the previous column by dividing by \sqrt{N} , where N is the number of measurements for a given galaxy.^h HI velocity dispersion measured from naturally weighted maps from Walter et al. (2008) over same area as the CO measurement.ⁱ From van der Kruit & Shostak (1982).

tween our sample and the THINGS sample (Walter et al. 2008), we can compare the velocity dispersions in the atomic and molecular gas directly. The moment 2 maps for the THINGS sample were produced using a slightly different masking technique (Walter et al. 2008) than the one we adopted for our CO analysis. In the THINGS processing, the data are first smoothed to a resolution of 30". A mask is then made keeping only those pixels and velocity channels (width either 2.6 or 5.2 km s⁻¹) where the emission exceeds 2 σ in 3 adjacent velocity channels. We used the natural weighted maps of the HI velocity dispersion and measure the dispersion over the same region in which the CO dispersions have been measured. These velocity dispersions are also given in Table 1. Note that these HI dispersions are somewhat larger than the typical value of 11 ± 3 km s⁻¹ given in Leroy et al. (2008) because they are measured in the inner rather than the outer disks of the galaxies.

3 VELOCITY DISPERSIONS IN THE MOLECULAR GAS DISK

The observed CO velocity dispersion maps are shown in Figures 1 and 2. Figures 3 and 4 show the observed velocity dispersion as a function of radius for the 12 galaxies in our

sample. Beam smearing is expected to have an effect only on the measured velocity dispersions for the central pixel in each plot. Three of the galaxies (NGC 628, NGC 2403, and NGC 3184) show very flat profiles as a function of radius. These late type spirals are also the least luminous and so presumably are also the least massive galaxies in our sample. The remaining 9 galaxies show a central peak in the velocity dispersion extending to 0.2 – 0.4 r_{25} . We attribute part of this increase to the effects of a steeply rising rotation curve at our relatively low (0.2-1.2 kpc) spatial resolution in these galaxies. Thus, for these galaxies, we measure the average velocity dispersion in the outer disk excluding a central circular region. The exclusion aperture was chosen by examining the individual velocity dispersion maps to identify the smallest aperture that would exclude the region of most obviously enhanced dispersion. We found that a diameter of 5.3 kpc (9 pixels or 65" at the distance of Virgo) worked well for all five galaxies in the Virgo cluster and that a similar physical region was appropriate for the other galaxies in our sample. However, the maps of NGC 4736 and NGC 4826 contain no data at larger radii, and so for these two galaxies we quote disk velocity dispersions excluding only a central 9 pixel diameter region. The disk velocity dispersions of these two galaxies are likely biased to be somewhat higher than those of the other galaxies in our sample and thus we do not

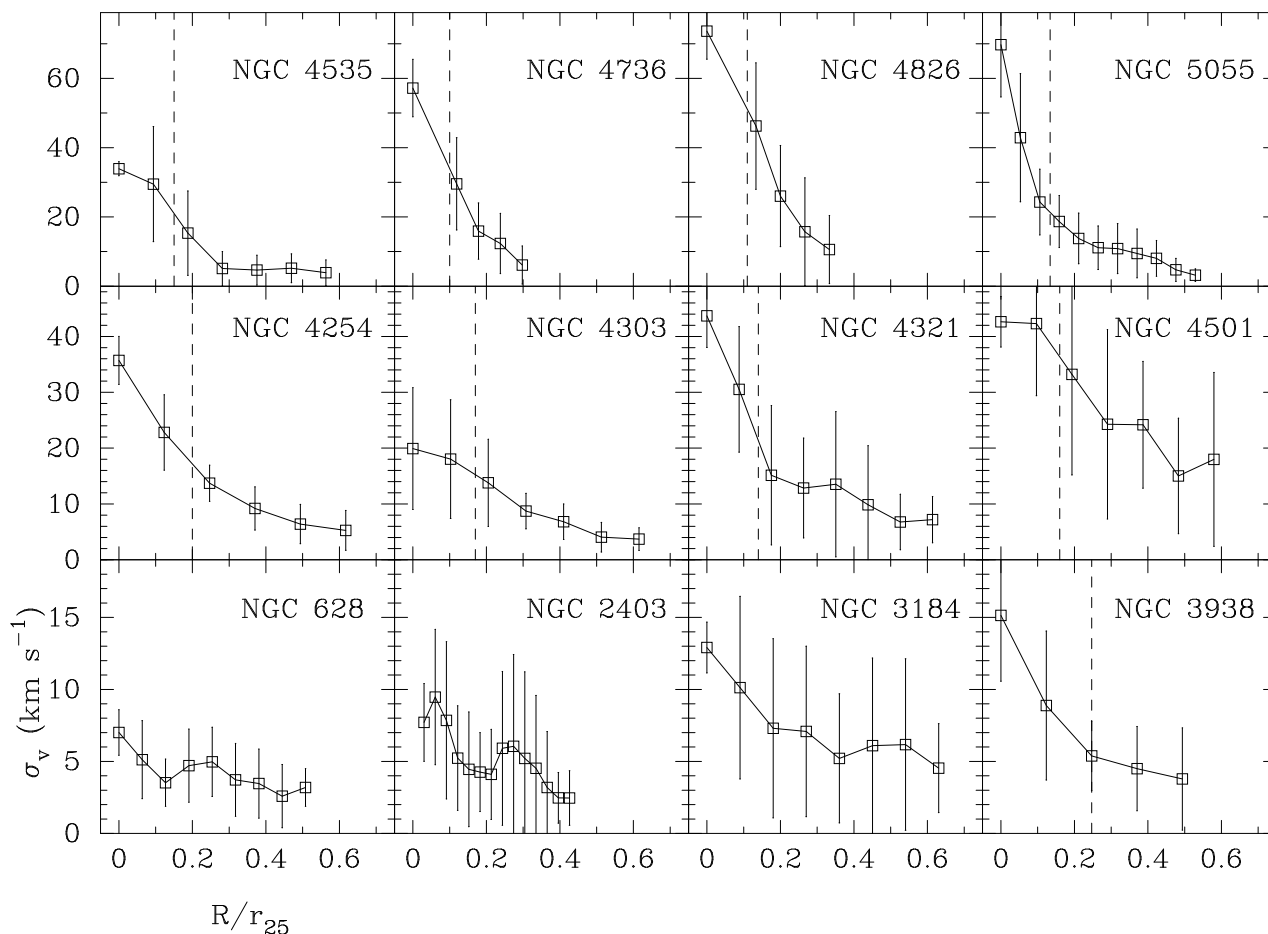


Figure 3. Observed CO $J=3-2$ velocity dispersion as a function of radius normalized by r_{25} . These velocity dispersions have not been corrected for any contribution from the internal velocity dispersion of individual giant molecular clouds (see text). Where appropriate, the central region excluded from calculating the disk-averaged velocity dispersion is indicated by the dashed line.

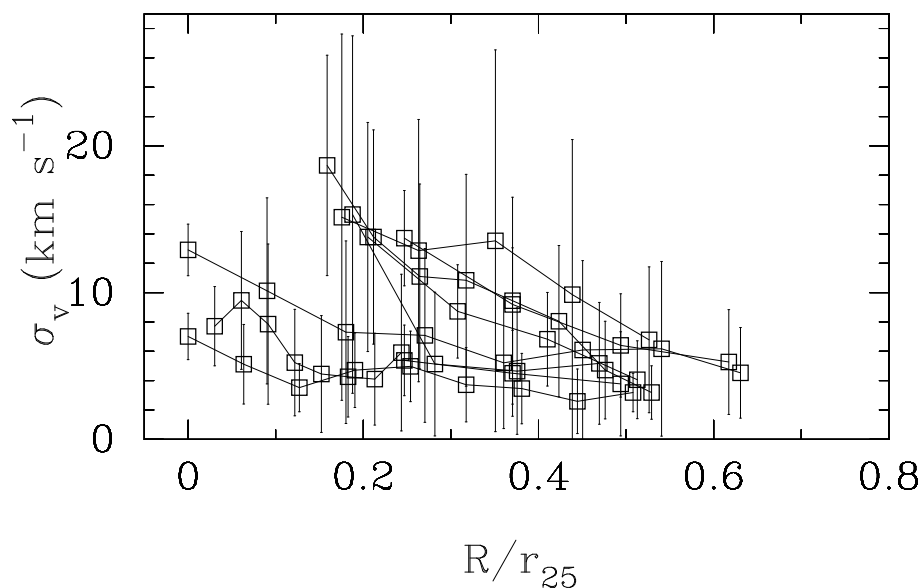


Figure 4. Observed CO $J=3-2$ velocity dispersion as a function of radius normalized by r_{25} , showing nine galaxies on a single plot. Data points with $r < 2.65$ kpc are not plotted for the 6 galaxies with central peaks in the velocity dispersion.

include them in calculating the average outer disk velocity dispersion.

The average observed velocity dispersions in the molecular gas measured for the 12 galaxies in our sample are given in Table 1. These velocity dispersions are consistent with previous measurements for the Milky Way (Stark & Brand 1989), M33, (Wilson & Scoville 1990) and other nearby galaxies (Combes & Bica 1997; Walsh et al. 2002). The observed velocity dispersion in the molecular gas disk ranges from a low of 4.1 km s⁻¹ in NGC 628 to a high of 20.1 km s⁻¹ in NGC 4501. We exclude NGC 4736 and NGC 4826 from our averages because we can only trace the velocity dispersions in the inner region where the profile is still rising steeply. We further exclude NGC 4501 because its very high velocity dispersion and evidence for double peaked line profiles in the north-west portion of the disk suggest that the molecular gas has been affected by the same ram pressure effects seen in HI (Vollmer et al. 2008). The average observed value for the remaining 9 galaxies is 7.1 ± 0.9 km s⁻¹ (standard deviation 2.6 km s⁻¹), 50% smaller than the average of 11 ± 3 km s⁻¹ measured for the atomic gas in the outer disks of spiral galaxies (Leroy et al. 2008). If we compare the atomic and molecular velocity dispersions in the same region of the disk (Table 1), the observed velocity dispersion in the molecular gas is on average ~ 2 times smaller than the dispersion in the atomic gas.

3.1 The effect of cloud internal velocity dispersions

The low values measured for the velocity dispersion, particularly for NGC 628 and NGC 3938, lead us to consider the effect of internal velocity dispersions of individual giant molecular clouds on the observed velocity dispersion. A second complicating effect, that of an anisotropy between the vertical and in-plane motions of the GMCs, would be expected to produce a correlation of velocity dispersion with inclination, which is not seen in our data (Figure B1). Nevertheless, we discuss the potential magnitude of this effect in Appendix B.

Individual giant molecular clouds have internal velocity dispersions that are substantially larger than the thermal line-widths expected for gas with physical temperatures of 10-30 K. In the study of Solomon et al. (1987), individual GMCs show internal velocity dispersions ranging from 1-8 km s⁻¹. These internal velocity dispersions are obtained from an intensity-weighted measure of the dispersion in radial velocity within a single cloud and thus are directly comparable (in technique) to the intensity-weighted dispersions averaged over the galactic disk presented here. What we need is an estimate of the contribution of the internal velocity dispersions of an ensemble of GMCs with a range of masses to the observed velocity dispersion in the disk. With this value, it is easy to show that the observed velocity dispersion, σ_v , is given by $\sigma_v^2 = \sigma_{c-c}^2 + \bar{\sigma}_{int}^2$ where $\bar{\sigma}_{int}$ is the mass-weighted average internal velocity dispersion for our ensemble of clouds and σ_{c-c} is the value we are interested in measuring, that is, the cloud-cloud velocity dispersion.

It is well known that the cloud internal velocity dispersion, σ_{int} , relates to the cloud mass as $M \propto \sigma_{int}^4$, as first proposed by Henriksen & Turner (1984). Observationally, Solomon et al. (1987) find that the internal velocity

dispersion σ_{int} (in km s⁻¹) relates to the cloud mass M (in M_⊙) as $M = 2000\sigma_{int}^4$. If we assume a cloud mass function $dN/dm \propto m^{-\alpha}$, then we can estimate the mass-weighted average internal velocity dispersion for an ensemble of clouds between M_{low} and M_{high} . Since column density is proportional to intensity for the CO lines (Strong et al. 1988), a mass-weighted average is also equivalent to an intensity-weighted average. The mass-weighted square of the internal velocity dispersion is then $\int m\sigma_{int}^2 dN / \int m dN$ which, using the relation between σ_{int} and M given by Solomon et al. (1987) and assuming $\alpha \neq 2$, reduces to

$$\overline{\sigma_{int}^2} = \frac{1}{44.7} \frac{2 - \alpha}{2.5 - \alpha} \frac{M_{high}^{2.5-\alpha} - M_{low}^{2.5-\alpha}}{M_{high}^{2-\alpha} - M_{low}^{2-\alpha}}$$

For $\alpha = 1.5$ (Sanders et al. 1985), $M_{high} = 10^6 M_{\odot}$ and $M_{low} = 10^4 M_{\odot}$ (e.g., Solomon et al. 1987), $\bar{\sigma}_{int} = 3.5$ km s⁻¹. The exact result clearly depends on the details of the model.

Interestingly, this estimate of the average cloud internal velocity dispersion is comparable to the value of 4.1 km s⁻¹ observed in the disk of NGC 628. The average CO $J=3-2$ intensity in NGC 628 of 0.8 K km s⁻¹ is the lowest intensity in our sample and translates into an average mass per JCMT beam of only $4 \times 10^6 M_{\odot}$. For a GMC mass function with slope $\alpha = 1.5$, this surface density translates into an average of just 10 clouds with $10^5 < M < 10^6 M_{\odot}$ per beam. This calculation suggests that, although the number of massive ($> 10^5 M_{\odot}$) GMCs per beam may be subject to small number statistics in NGC 628, their effect on the velocity dispersion should be observable on average if such large clouds are present in NGC 628. This analysis suggests that NGC 628 is likely deficient the largest molecular clouds; if we instead limit the maximum cloud mass to $10^5 M_{\odot}$, then the mass-weighted average internal velocity dispersion reduces to $\bar{\sigma}_{int} = 2.2$ km s⁻¹. The larger average integrated intensities and observed velocity dispersions suggests that the molecular cloud mass spectrum is likely to be fully populated in the remaining galaxies in our sample. Thus, in correcting the observed velocity dispersions for the effects of internal cloud velocity dispersions, we use a value for $\bar{\sigma}_{int}$ of 2.2 km s⁻¹ for NGC 628 and 3.5 km s⁻¹ for the rest of the sample. The corrected values for the cloud-cloud velocity dispersion are given in Table 1 along with the uncertainty in the mean cloud-cloud velocity dispersion for each galaxy. The uncertainty in the mean has been calculated assuming that the errors are normally distributed, so that the uncertainty in the mean is given by the standard deviation divided by \sqrt{N} , where N is the number of measurements for a given galaxy.

3.2 The true vertical velocity dispersion of the molecular gas

Based on the discussion in the previous section, the observed velocity dispersion includes both a contribution from the internal velocity dispersion of individual giant molecular clouds as well as a contribution from the cloud-cloud velocity dispersion. It is this second quantity, the cloud-cloud velocity dispersion, which is of interest for determining the molecular gas scale height, analysing the stability of the gas disk, etc. The small observed velocity dispersions imply that the

correction for the internal velocity dispersion of the clouds is not negligible. Correcting for the average internal cloud velocity dispersion as discussed in §3.1 gives measures of the cloud-cloud velocity dispersions which range from 2.7 to 19.8 km s⁻¹. Again excluding NGC 4501, NGC 4736, and NGC 4826, we obtain an average value of 6.1 ± 1.0 km s⁻¹ (standard deviation 2.9 km s⁻¹).

4 DISCUSSION

4.1 Molecular and atomic gas velocity dispersions

The average cloud-cloud velocity dispersion in the molecular gas in this group of spiral galaxies of 6.1 ± 1.0 km s⁻¹ is slightly smaller than previous estimates for external galaxies which did not take the effect of internal cloud dispersion into account (Combes & Becquaert 1997; Walsh et al. 2002), but is comparable to recent measurements for the cloud-cloud dispersion of massive clouds in the Galaxy (Stark & Lee 2006) and in M33 (Wilson & Scoville 1990).

4.1.1 Effects of CO optical depth

An additional possible concern in interpreting the CO data is the high optical depth of the CO line. Since we are interested in the cloud-cloud velocity dispersion, it is important to check whether the surface density of the molecular gas is sufficiently high that shielding of one cloud by another at a similar velocity could affect our measurements. For all but one of the galaxies in our sample, the projected surface density N_H is substantially smaller than the typical surface density of individual giant molecular clouds ($N_H = 1.5 \pm 0.3 \times 10^{22}$ cm⁻², McKee 1989), and thus cloud-cloud shielding is unlikely to be a problem. Only in NGC 4736, where the surface density may be as high as 3×10^{22} cm⁻² (assuming a CO J=3-2/J=1-0 line ratio of 0.3 and a CO to H₂ conversion factor of 2×10^{20} cm⁻² (K km s⁻¹)⁻¹ Strong et al. 1988), is it possible the clouds may shield one another to some degree. However, the actual surface density depends sensitively on the value that we assume for the CO J=3-2/J=1-0 line ratio; if we adopt a value of 0.6 which is more appropriate for the dense gas, rather than the value of 0.3 found in a direct comparison of CO J=3-2 and J=1-0 maps of NGLS galaxies (Wilson et al. 2009; Warren et al. 2010), then the projected disk-averaged column density is similar to that of individual GMCs. Thus, we conclude that we can ignore the possibility of cloud-cloud shielding in the disks of the galaxies in this sample.

4.1.2 Observed HI velocity dispersions

Combes & Becquaert (1997) showed that the molecular and atomic components in NGC 628 and NGC 3938 had vertical velocity dispersions that are similar to each other and virtually constant with radius. As a consequence, the authors suggested that the two layers had similar scale heights and that HI and H₂ simply represent different phases of the same dynamical component. It is clear, however, from observations of our own Milky Way as well as edge-on galaxies that the molecular disk is significantly thinner than the HI disk. Our observed velocity dispersions are comparable to

those found by Combes & Becquaert (1997), although we have shown that it is necessary to correct for internal velocity dispersion to determine the cloud-cloud velocity dispersion that is relevant for scale height determinations. For HI, on the other hand, we know that its stable phases occur in both hot diffuse gas as well as colder clouds (the warm neutral medium and cold neutral medium, respectively). Although discrete HI clouds are identifiable in our Galaxy (see Lockwood 2001; Stil et al. 2006), the clouds are smaller and warmer than molecular clouds. Because of the admixture of cool and warm HI components over the size scale of the beam in external galaxies, similar corrections need not be applied to the HI velocity dispersions. Also, since the HI is a diffuse collisional medium, its velocity dispersion is assumed to be isotropic (e.g. Malhotra 1995). We have therefore compared the observed HI dispersion directly with our cloud-cloud velocity dispersion derived from the CO data.

4.1.3 Comparing CO and HI velocity dispersions

The published HI velocity dispersion map for NGC 4501 (Vollmer et al. 2008) shows velocity dispersions in the range of 10-20 km s⁻¹ across the extended disk, comparable to the cloud-cloud velocity dispersion (Table 1) over the same area. High resolution HI data have been published for NGC 4321 (Knapen et al. 1993) and NGC 4254 (Phookun et al. 1993), but the velocity dispersion maps are not presented; we could find no published high resolution HI data for NGC 4303 and NGC 4535. An older measurement of the HI velocity dispersion of 10 km s⁻¹ for NGC 3938 (van der Kruit & Shostak 1982) is roughly 3 times larger than our derived cloud-cloud velocity dispersion.

We have compared the velocity dispersions in the molecular and atomic gas measured over the same regions for six galaxies in our sample for which maps of the atomic gas velocity dispersion are available from the THINGS sample (Walter et al. 2008). On average, the cloud-cloud velocity dispersion determined from CO data is roughly half that of the atomic gas. The exception to this trend is NGC 4826, for which the cloud-cloud velocity dispersion is a factor of 5 times smaller than the the HI velocity dispersion. However, this galaxy has quite a steep radial gradient in the observed velocity dispersion (Figure 3) and so the average disk value depends sensitively on what aperture is used. Overall, these results imply that the scale height of the molecular gas is roughly half that of the atomic gas. This estimate of the ratio of the scale heights is roughly consistent with the estimate of the relative HI and CO scale heights in the Milky Way as discussed in Combes & Becquaert (1997). We should note, however, that narrow (4-5 km s⁻¹) HI line components have been seen in a few Local Group dwarf galaxies observed with high spatial resolution (Young & Lo 1996, 1997; de Blok & Walter 2006). These narrow lines, which may represent atomic gas cooling to form the precursors of GMCs, are typically superimposed on a broader underlying line which likely represents the overall warm neutral atomic medium.

4.2 Correlations with other global properties

The infrared luminosity is a useful tracer of the star formation activity within a galaxy (Kennicutt 1998). Enhanced

star formation might be expected to increase the velocity dispersion in the interstellar medium via stellar winds and supernova explosions. Indeed, Tamburro et al. (2009) find evidence that supernovae linked to recent star formation are important for maintaining the velocity dispersion in the atomic gas. We find a statistically significant correlation (95% confidence level) of both the observed and the cloud-cloud velocity dispersion with infrared luminosity (Sanders et al. 2003) for the 9 galaxies in our sample. Thus, like the atomic gas, there is some evidence for star formation activity enhancing the velocity dispersion in the dense molecular gas. We also find a statistically significant correlation (95% confidence level) of both the observed and the cloud-cloud velocity dispersion with the absolute K-band and absolute B-band magnitude (Jarrett et al. 2003). Assuming the K-band magnitude traces the total stellar mass, this correlation suggests that the cloud-cloud velocity dispersion is enhanced in more massive galaxies. For all these correlations, however, it is important to keep in mind that we have compared the average velocity dispersion in the disk (excluding the central regions) with a global luminosity which would include the contribution from the central regions.

There also appears to be a dependence in our sample of the velocity dispersion on galaxy morphology. We divided our sample into early (type ab-bc) and late (type c-cd) spirals and calculated the average velocity dispersion for each sub-sample. The average observed dispersion for 6 late-type spirals is $5.8 \pm 0.3 \text{ km s}^{-1}$, while the value for 3 early-type spirals is $9.7 \pm 0.6 \text{ km s}^{-1}$. These two values differ at the 6 sigma level. Of course, this dependence on morphology could be tracing some other variable in our sample, such as mass or star formation activity. In fact, the average infrared luminosities differ by a factor of three between the early- and late-type samples, while the K-band luminosity differs by a factor of four. Thus, it seems most likely that the dependence on morphology is driven by differences in the average star formation rates and masses between the early and late type samples.

4.3 Disk stability and star formation laws

The velocity dispersion of the interstellar medium is an important parameter in understanding the stability of galactic disks against gravitational collapse. Jog & Solomon (1984a,b) showed that a rotating disk composed of two fluids with different surface densities and velocity dispersions can be unstable to perturbations even if each fluid disk is stable on its own. They also showed that a galaxy must be treated as a two fluid system when the colder gaseous component comprises as little as 10% of the total mass of the system. Treating the stellar component as a collisional fluid, they found that the critical velocity dispersion required for stability in this higher dispersion system is larger in the presence of a second cold fluid than if the stellar system is treated in isolation. Rafikov (2001) considered the case of a single fluid and multiple collisionless (stellar) components, but found that the stability conditions were quite similar in the two fluid case whether or not the stellar component was treated as collisionless.

Yang et al. (2007) applied the approach of Rafikov (2001) to compare the location of star forming regions in the

Large Magellanic Cloud (LMC) with the disk stability criterion. They adopted a gas velocity dispersion of 5 km s^{-1} , very similar to the value found in our sample of spiral galaxies. They found that there was a much better spatial correlation of star forming regions with regions where the disk was unstable when instability was evaluated using the contribution of both the gas and the stars. Leroy et al. (2008) applied the two collisional fluid equation of Rafikov (2001) to a number of galaxies in the THINGS sample (Walter et al. 2008). They adopted a gas velocity dispersion of 11 km s^{-1} from measurements of the HI component. Similarly to Yang et al. (2007), they found that the Q values were smaller when both the stars and the gas were included in the analysis; however, they found that the disks were globally stable against large scale perturbations.

The results for the molecular velocity dispersion presented here imply that the interstellar medium in spiral galaxies is itself a multi-fluid system, with the molecular gas disk being dynamically significantly colder than the atomic gas disk. Since previous analyses have found that the colder of the two components has the larger effect on the disk stability (Jog & Solomon 1984a), it seems likely that, if we were to use one phase of the ISM in our stability analysis, it should be the dynamically coldest phase, which is the molecular gas. This would be especially true for the inner regions of those spiral disks where the ISM mass is predominantly H_2 . The Toomre Q parameter for the combined system tends to decrease as the velocity dispersion of the coldest (gas) component decreases and as the gas mass fraction ($\Sigma_{\text{gas}}/\Sigma_*$) increases (Jog & Solomon 1984b; Rafikov 2001). This effect suggests that the Q values derived by Leroy et al. (2008) are likely to be significantly larger than the values that would be derived if the molecular gas values for surface density and velocity dispersion were used in the analysis, a possibility that was discussed in Leroy et al. (2008) as well. It would be informative to repeat the stability analysis for the galaxies in common between our sample and the THINGS sample to see if the disks remain globally stable as judged by the Q parameter when the cloud-cloud velocity dispersion of the molecular gas is included. We plan to investigate this issue further in a future paper.

The need to treat the ISM itself as a multi-fluid system suggests that we may not be able to separate the discussion of the instabilities in the atomic and molecular phases. For example, we might imagine that the Q value for the atomic gas governs the formation of molecular clouds from the HI disk, while the star formation from those clouds would then be governed by the Q value for the molecular disk. However, the two fluid analysis by Jog & Solomon (1984a) and Rafikov (2001) implies that the Q value and hence the stability properties of the atomic disk are affected by the presence of the dynamically colder molecular disk. In particular, an atomic gas disk with a stable value of Q when considered in isolation might be found to be unstable when the presence of a relatively small quantity of molecular gas is included. Of course, a complete analysis would include the properties of the stellar disk (perhaps multiple components, as in Rafikov 2001) in addition to the two fluid components of the ISM. Such an analysis is beyond the scope of this paper.

4.4 Implications for turbulent support of the ISM

The scale height of a gaseous component in hydrostatic equilibrium depends on both gravitational and pressure gradients. Gravitational gradients originate in the disk as well as a dark matter halo potential. The pressure will include internal thermal pressure, turbulent pressure and, if important, pressure due to cosmic rays and magnetic fields. At the radius of the Sun in the Milky Way, the magnetic and cosmic ray pressures supply about half of the total pressure and the thermal and turbulent pressures supply the remaining half (Hanasz & Lesch 2004). At the temperatures of the molecular components, turbulent pressure dominates over thermal pressure within and between clouds (e.g. Brunt 2003). In the HI, thermal pressure likely dominates in the Warm Neutral Medium whereas both may be important for the Cold Neutral Medium (Heiles & Troland 2003). Measured velocity dispersions can only probe the dynamical components (thermal and turbulent) and therefore can only predict the scale height of the gas provided that the dynamical components dominate over the magnetic and cosmic ray pressures and provided that the disk ISM is in pressure equilibrium.

Star formation activity is typically associated with heating sources and sources of turbulence through supernovae and stellar winds. Most of the galaxies in our sample show a radial decline in the CO velocity dispersion (Figure 4). The velocity dispersion in HI is also a declining function of radius (Tamburro et al. 2009), although HI disks retain significant velocity dispersions outside any star forming disk (e.g. Sellwood & Balbus 1999; Tamburro et al. 2009). Tamburro et al. (2009) found a good correlation between the kinetic energy of the HI and the star formation rate and suggest that supernovae are likely sufficient to maintain the HI velocity dispersion in regions with significant star formation. The correlation of the cloud-cloud velocity dispersion with the star formation rate as traced by the infrared luminosity suggests that star formation may also be the dominant source of turbulence in the H₂-rich parts of spiral disks.

However, some galaxies do show a lack of correlation between turbulence in the atomic gas and star formation as a function of radius. (e.g. Dickey et al. 1990; van Zee & Bryant 1999; Petric & Rupen 2007). The three lowest luminosity galaxies in our sample show a roughly constant cloud-cloud velocity dispersion as a function of radius (see also Combes & Bequaert 1997). These results suggest that non-thermal energy input in the form of turbulence that is unrelated to star formation may be important for understanding the vertical velocity dispersions in disks. Magnetic instabilities may be the most promising source of turbulence. Parker instabilities (Parker 1966) are well-known, but seem to require cosmic rays from supernovae as triggers to be most effective (Hanasz & Lesch 2000). Thus, Parker instabilities cannot account for the observed dispersions seen outside of the active star forming disk, but could be important for the inner molecular disks where star formation is occurring. Another possibility is the Balbus-Hawley (or magneto-rotational) instability (Balbus & Hawley 1991, 1998), or other instabilities related to magnetic stresses (e.g. Sellwood & Balbus 1999). Tamburro et al. (2009) suggest that a combination of thermal broadening and magneto-rotational instabilities can account for the HI velocity dispersion beyond r_{25} . Simulations of the magneto-rotational

instability by Piontek & Ostriker (2007) for the two-phase HI component have shown that the turbulent velocity amplitude varies as $\propto n^{-0.77}$, where n is the mean density of the component. If this turbulence is dominant in both molecular and atomic gas, then the difference in velocity dispersion between the two components may simply relate to their respective densities.

4.5 Disk galaxies at high redshift

Observations of the molecular gas content in galaxies at redshifts $z = 1 - 3$ are often made using the CO J=3-2 line, which at these redshifts falls into the standard millimetre observing windows. Most high-resolution detections of high redshift galaxies are unusually luminous systems, such as submillimetre galaxies (Tacconi et al. 2008) or quasars (Coppin et al. 2008). Although many of these high redshift detections appear as simple point sources at current resolution limits, there are a few systems for which we can begin to resolve the velocity structure. Even more interesting from the point of view of this paper are the observations of more normal galaxies at redshifts 1-1.5, which are becoming available (Daddi et al. 2008; Dannerbauer et al. 2009; Daddi et al. 2010; Tacconi et al. 2010). These galaxies are found to be quite extended (~ 10 kpc), significantly more so than the quasars and submillimeter galaxies (Daddi et al. 2010; Tacconi et al. 2010). Given the sensitivity and wide field of view of our observations, it is interesting to examine how our galaxies would appear if placed at a redshift of 1.

We have processed a subset of our galaxies to see what changes are produced in an analysis of the velocity dispersion when the spatial resolution of the data is degraded. For three of the brightest galaxies in the Virgo Cluster (NGC 4254, NGC 4321, and NGC 4303), we convolved the baseline-subtracted data cube with a $54''$ gaussian to achieve an effective beam of $56''$ or 4.5 kpc at a distance of 16.7 Mpc. We then constructed moment maps from the smoothed data cube using the methods described in § 2. A comparison of the resulting velocity dispersion maps for NGC 4254 is shown in Figure 5. Depending on how much of the central high dispersion regions is excluded from the analysis, the average velocity dispersion in the outer disk of the low resolution image is on average twice as large as the value in the high resolution image. Similar increases of about a factor of two in the average velocity dispersion in the disk are seen for NGC 4321 and NGC 4303. The images also suggest that a plot of velocity dispersion as a function of radius would yield higher values at a given radius in the low resolution image. These effects of resolution will need to be taken into account as we begin to accumulate data on the dense molecular gas properties in galaxies at high redshift.

The average values of 20-30 km s⁻¹ seen at low resolution in the disks of these three galaxies are quite similar to the value of ~ 20 km s⁻¹ found in EGS13035123 by Tacconi et al. (2010). EGS13035123 has 10-20 times the star formation rate, H₂ gas mass, and stellar mass compared to NGC 4254 (Kennicutt et al. 2003; Wilson et al. 2009; Kranz et al. 2003). However, EGS13035123 is also roughly a factor of three larger in its CO radius than NGC 4254 (Wilson et al. 2009), which implies that the gas surface density, stellar surface density, and star formation rate surface density inside the molecular disks of these two galaxies are

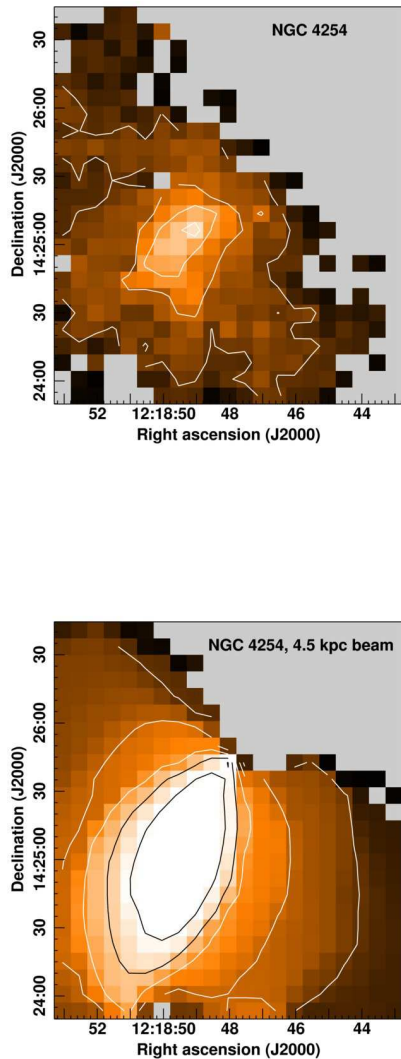


Figure 5. (a) CO $J=3-2$ velocity dispersion for NGC 4254 at the native resolution of the JCMT data ($14.5''$ or 1.15 kpc at a distance of 16.7 Mpc). Colour scale runs from 0 to 60 km s^{-1} and the contours are 10, 20, 30, 40, 50 km s^{-1} . (b) CO $J=3-2$ velocity dispersion for NGC 4254 smoothed to a resolution of 4.5 kpc ($56''$) to match the resolution of observations of disk galaxies at $z \sim 1$ of Tacconi et al. (2010). Colour scale and contours are the same as in (a).

quite similar. Thus, the similar velocity dispersions between the two galaxies are likely related to the similar mass surface densities in the disk. The two galaxies also have quite similar molecular gas fractions of ~ 0.25 (Tacconi et al. 2010; Wilson et al. 2009; Kranz et al. 2003). This comparison supports a picture where the high star formation rates seen at $z = 1$ may be at least partly due to the presence of physically larger molecular gas disks at this epoch.

5 CONCLUSIONS

We have used large-area high velocity resolution CO $J=3-2$ observations of 12 nearby galaxies to study the vertical velocity dispersion in the dense molecular gas. Three of the galaxies show a roughly constant velocity dispersion as a function of radius, while the other nine galaxies have a central peak followed by a fall-off with radius to typically $0.2 - 0.4r_{25}$. Flat velocity dispersion profiles are seen only in some of the late-type spiral galaxies in our sample, and those with flat profiles have the lowest mass. The observed values of the velocity dispersion range from 4.1 km s^{-1} to 20.1 km s^{-1} . These velocity dispersions are comparable to the internal velocity dispersions of individual giant molecular clouds in our own and other galaxies (Solomon et al. 1987; Wilson & Scoville 1990). Correcting for these internal velocity dispersions yields an average cloud-cloud velocity dispersion of $6.1 \pm 1.0 \text{ km s}^{-1}$ measured over 9 galaxies with good radial profiles. This cloud-cloud velocity dispersion is comparable to recent measurements in our own Galaxy (Stark & Lee 2005, 2006) and M33 (Wilson & Scoville 1990).

A direct comparison with the high resolution HI maps from the THINGS survey (Walter et al. 2008) in six galaxies show that the cloud-cloud velocity dispersion is on average twice as small as the velocity dispersion of the atomic gas, which implies a much smaller scale height for the molecular gas. Theoretical analyses of the stability of multi-component disks suggest that the dynamically coldest component is the most important in driving instability (Jog & Solomon 1984a,b; Rafikov 2001). This analysis suggests that it is the properties of the dense molecular gas, rather than the atomic gas, that are the most important for determining whether galactic disks are stable against gravitational collapse, especially where the mass of the ISM is H_2 dominated.

The cloud-cloud velocity dispersion is correlated at the 95% confidence level with both the far-infrared luminosity and the K-band absolute magnitude. Thus, as for the atomic gas, we find evidence that star formation activity (as traced by the infrared luminosity) tends to increase the velocity dispersion in the dense molecular gas. The correlation with K magnitude, which traces the total stellar mass, implies that the cloud-cloud velocity dispersion is also enhanced in more massive galaxies.

We have used our data to examine the apparent kinematical properties of the molecular disk at a spatial resolution of 4.5 kpc chosen to match the best resolution for galaxies at redshifts 1-2 (Tacconi et al. 2008). A degradation of the resolution from 1.2 kpc to 4.5 kpc results in an increase in the average velocity dispersion in the outer disk by a factor of two. The average velocity dispersion of NGC 4254 viewed with 4.5 kpc resolution is quite comparable to the velocity dispersion of 20 km s^{-1} seen in a normal galaxy at $z = 1$ (Tamburro et al. 2009). Both galaxies have comparable gas and stellar surface densities, as well as star formation rate surface densities, which suggests that the higher star formation rates seen at $z = 1$ may be partly attributed to the presence of physically larger molecular disks. This analysis suggests that this data set can provide a valuable local benchmark in understanding lower spatial resolution observations of galaxies in the early universe.

ACKNOWLEDGMENTS

We thank the anonymous referee for a referee report which spurred us to re-examine our data processing choices and resulted in a significant improvement in the paper. The James Clerk Maxwell Telescope is operated by The Joint Astronomy Centre on behalf of the Science and Technology Facilities Council of the United Kingdom, the Netherlands Organisation for Scientific Research, and the National Research Council of Canada. The research of J.I. and C.D.W. is supported by grants from NSERC (Canada). A.U. has been supported through a Post Doctoral Research Assistantship from the UK Science & Technology Facilities Council. Travel support for B.E.W. and T.W. was supplied by the National Research Council (Canada). We acknowledge the usage of the HyperLeda database (<http://leda.univ-lyon1.fr>) and thank R.N. Henriksen for useful discussions. This research has made use of the NASA/IPAC Extragalactic Database (NED) which is operated by the Jet Propulsion Laboratory, California Institute of Technology, under contract with the National Aeronautics and Space Administration.

REFERENCES

Balbus, S. A. & Hawley, J. F. 1991, *ApJ*, 376, 214
 Balbus, S. A. & Hawley, J. F. 1998, *Rev. Mod. Phys.* 70, 1
 Berry, D. S., Reinhold, K., Jenness, T., & Economou, F., 2007, in *Astronomical Data Analysis Software and Systems XVI*, ASP Conference Series, Vol. 376, eds. R. A. Shaw, F. Hill & D. J. Bell., 425
 Bigiel, F., Leroy, A. K., Walter, F., Brinks, E., de Blok, W. J. G., Madore, B., & Thornley, M. D., 2008, *AJ*, 136, 2846
 Brunt, C. 2003, *ApJ*, 583, 280
 Buckle, J. V., et al., 2009, *MNRAS*, 399, 1026
 Buta, R. J., Corwin, H. G., Odewahn, S. C. 2007, *The de Vaucouleurs Atlas of Galaxies* (Cambridge: Cambridge University Press)
 Calzetti, D. et al. 2007, *ApJ*, 666, 870
 Cayatte, V., van Gorkom, J. H., Balkowski, C., & Kotanyi, C., 1990, *AJ*, 100, 604
 Clemens, D. P., 1985, *APJ*, 295, 422
 Combes, F. & Becquaert, J.-F., 1997, *A&A*, 327, 453
 Coppin, K. E. K., et al. 2008, *MNRAS*, 389, 45
 Currie, M. J., Draper, P. W., Berry, D. S., Jenness, T., Cavanagh, B., & Economou, F., 2008, in *Astronomical Data Analysis Software and Systems*, ASP Conference Series, Vol. 394, eds. R. W. Argyle, P. S. Bunclark, & J. R. Lewis, 650
 Daddi, E., Dannerbauer, H., Elbaz, D., Dickinson, M., Morrison, G. E., Stern, D., & Ravindranath, S., 2008, *ApJ*, 673, L21
 Dannerbauer, H., Daddi, E., Riechers, D. A., Walter, F., Carilli, C. L., Dickinson, M., Elbaz, D., & Morrison, G. E. 2009, *ApJ*, 698, L178
 Daddi, E., et al., 2010, *ApJ*, 714, 118
 de Blok, W. J. G. & Walter, F. 2006, *AJ*, 131, 363
 de Blok, W. J. G., Walter, F., Brinks, E., Trachternach, C., Oh, S.-H., & Kennicutt, R. C., 2008, *AJ*, 136, 2648
 Delhaye, J., 1965, in *Galactic Structure*, Eds. A. Blaauw & M. Schmidt, University of Chicago Press, 61

Dehnen, W., & Binney, J., 1998, *MNRAS*, 298, 387
 Dickey, J. M., Hanson, M. M., & Helou, G. 1990, *ApJ*, 352, 522
 Dickey, J. 2009a, arXiv:0901.2380v1
 Dickman, R. L., Snell, R. & Schloerb, F. P. 1985, *ApJ*, 309, 326
 Freedman, W. L., et al., 2001, *ApJ*, 553, 47
 Elias, F., Alfaro, E. J., & Cabrera-Caño, J., 2006, *AJ*, 132, 1052
 Gammie, C. F., Ostriker, J. P., & Jog, C. J., 1991, *ApJ*, 378, 565
 García-Burillo, S., Combes, F., & Gerin, M., 1993, *A&A*, 274, 148
 Hanasz, M., & Lesch, H. 2000, *ApJ*, 543, 235
 Heiles, C., & Troland, T. H. 2003, *ApJ*, 586, 1067
 Henriksen, R. N. & Turner, B. E. 1984, *ApJ*, 287, 200
 Jarrett, T. H., Chester, T., Cutri, R., Schneider, S. E. & Huchra, J. P., 2003, *AJ*, 125, 525
 Jog, C. J., & Ostriker, J. P., 1988, *ApJ*, 328, 404
 Jog, C. J., & Solomon, P. M. , 1984, *ApJ*, 276, 114
 Jog, C. J., & Solomon, P. M. , 1984, *ApJ*, 276, 127
 Karachentsev, I. D., Karachentseva, V. E., Huchtmeier, W. K., & Makarove, D. I., 2004, *AJ*, 127, 2031
 Kenney, J. D. P. & Young, J. S., 1989, *ApJ*, 344, 171
 Kennicutt, R. C., 1989, *ApJ*, 344, 685
 Kennicutt, R. C. 1998, *ARA&A*, 36, 189
 Kennicutt, R. C. et al. 2003, *PASP*, 115, 928
 Kennicutt, R. C. et al. 2007, *ApJ*, 671, 333
 Knapen, J. H., Cepa, J., Beckman, J. E., del Rio, M. S., & Pedlar, A., 1993, *ApJ*, 416, 463
 Koopman, R. A., Kenney, J. D. P., & Young, J. S. 2001, *ApJS*, 135, 125
 Kranz, T., Slyz, A., & Hans-Walter Rix, H.-W., 2003, *ApJ*, 586, 143
 Larson, R. B., Tinsley, B. M., & Caldwell, C. N. 1980, *ApJ*, 237, 692
 Leonard, D. C., et al., 2002, *AJ*, 124, 2490
 Leroy, A. K., Walter, F., Brinks, E., Bigiel, F., de Blok, W. J. G., Madore, B., & Thornley, M. D., 2009, *AJ*, 136, 2782
 Lockwood, F. J. 2001, *ApJ*, 580, L47
 Malhotra, S. 1995, *ApJ*, 448, 138
 Maloney, P. & Black, J. 1988, *ApJ*, 325, 389
 McKee, C. F., 1989, *ApJ*, 345, 782
 Mei, S., et al. 2007, *ApJ*, 655, 144
 Mould, J. R., et al. 2000, *ApJ*, 529, 786
 Parker, E. N. 1966, *ApJ*, 145, 811
 Paturel, G., Fang, Y., Garnier, R., Petit, C., & Rousseau, J., 2000, *A&AS*, 146, 19
 Petric, A. O., & Rupen, M. P. 2007, *AJ*, 134, 1952
 Phookun, B., Vogel, S. N., & Mundy, L. G., 1993, *ApJ*, 418, 113
 Piontek, R. A., & Ostriker, E. C., 2007, *ApJ*, 663, 183
 Rafikov, R. R., 2001, *MNRAS*, 323, 445
 Sanders, D. B., Scoville, N. Z., & Solomon, P. M., 1985, *ApJ*, 289, 373
 Sanders, D. B., Mazzarella, J. M., Kim, D.-C., Surace, J. A., & Soifer, B. T., 2003, *AJ*, 126, 1607
 Sellwood, J. A., & Balbus, S. A. 1999, *ApJ*, 511, 660
 Solomon, P. M., Rivolo, A. R., Barrett, J., & Yahil, A., 1987, *ApJ*, 319, 730
 Stark, A. A., 1984, *ApJ*, 281, 624

Stark, A. A., & Brand, J., 1989, ApJ, 339, 763
 Stark, A. A., & Lee, Y., 2005, ApJ, 619, L159
 Stark, A. A., & Lee, Y., 2006, ApJ, 641, L113
 Stil, J. M., et al. 2006, ApJ, 637, 366
 Strong, A. W., et al. 1988, A&A, 207, 1
 Tacconi, L. J., et al. 2008, ApJ, 680, 246
 Tacconi, L. J., et al., 2010, Nature, 463, 781
 Tamburro, D.; Rix, H.-W., Walter, F., Brinks, E., de Blok, W. J. G., Kennicutt, R. C., & MacLow, M.-M., 2008, AJ, 136, 2872
 Tamburro, D., Rix, H.-W., Leroy, A. K., Low, M.-M. Mac, Walter, F., Kennicutt, R. C., Brinks, E., & de Blok, W. J., 2009, AJ, 137, 4424
 Tasker, E. J., & Tan, J. C., 2009, ApJ, 700, 358
 Thomasson, M., Donner, K. J., & Elmegreen, B. G., 1991, A&A, 250, 316
 Tonry, J. L, Dressler, A., Blakeslee, J. P., Ajhar, E. A., Fletcher, A. B., Luppino, G. A., Metzger, M. R., & Moore, C. B., 2001, ApJ, 546, 681
 Toomre, A., 1964, ApJ, 139, 1217
 van der Kruit, P. C. & Shostak, G. S., 1982, A&A, 105, 351
 van Zee, L., & Bryant, J. 1999, AJ, 118, 2172
 Vollmer, B., Soida, M., Chung, A., van Gorkum, J. H., Otmianowska-Mazur, K., Beck, R., Urbanik, M., and Kenney, J. D. P., 2008, A&A, 483, 89
 Walsh, W., Beck, R., Thuma, G., Weiss, A., Wielebinski, R., & Dumke, M., 2002, A&A, 388, 7
 Walter, F., Brinks, E., de Blok, W. J. G., Bigiel, F., Kennicutt, R. C., Thornley, M. D., & Leroy, A. K., 2008, AJ, 136, 2563
 Warren, B. E., et al., 2010, ApJ, 714, 571
 Williams, J. P., de Geus, E. J., & Blitz, L. 1994, ApJ, 428, 693
 Wilson, C. D., et al., 2009, ApJ, 693, 1736
 Wilson, C. D. & Scoville, N. Z., 1990, ApJ, 363, 435
 Yang, C.-C., Gruendl, R. A., Chu, Y.-H., Mac Low, M., & Fukui, Y., 2007, ApJ, 671, 374
 Young, J. S. & Scoville, N. Z. 1991, ARAA, 29, 581
 Young, J. S., et al., 1995, ApJS, 98, 219
 Young, L. M. & Lo, K. Y., 1997, ApJ 490 710
 Young, L. M. & Lo, K. Y., 1996, ApJ, 462, 203

APPENDIX A: COMPARISON WITH PREVIOUS PROCESSING METHODS

There are two different methods that have been used to measure velocity dispersions in molecular gas in galaxies. Combes & Becquaert (1997) measured velocity dispersions in NGC 628 and NGC 3938 by fitting gaussian profiles to individual spectra, while Walsh et al. (2002) used moment 2 maps of NGC 6946 to determine the average velocity dispersion. While the moment 2 maps used in this paper are easier to compute and analyse than fitting individual profiles to many hundreds of spectra, they can potentially be subject to some systematic effects depending on choices made in the processing. We investigate some of these effects here by comparing our data and moment 2 maps for NGC 628 and NGC 3938 with the results given by Combes & Becquaert (1997) for the same galaxies.

We first investigated whether the measured velocity dispersion was affected by the angular and spectral resolution

Table A1. Velocity dispersions measured with different spectral and spatial resolutions

Data cube used ^a	NGC 3938	NGC 628
Original	3.7	3.1
Binned to 2.6 km s ⁻¹	4.8	3.9
Convolved to 23'' gaussian	6.5	4.2
Convolved and binned	7.4	4.7
Combes & Becquaert (1997)	9	6.5

^a All values measured for the CO J=3-2 line in km s⁻¹.

Velocity dispersion measured using a signal-to-noise cutoff of 3.5 σ .

Table A2. Velocity dispersions measured with different signal-to-noise cutoffs for mask

S/N cutoff used ^a	NGC 3938	NGC 628
5 σ	3.8	3.4
4.5 σ	4.8	3.7
4.0 σ	5.7	3.9
3.5 σ	6.5	4.2
3.0 σ	7.2	4.6
2.5 σ	9.1	5.3
Combes & Becquaert (1997)	9	6.5

^a All values measured for the CO J=3-2 line in km s⁻¹.

of the data. The CO J=1-0 data from Combes & Becquaert (1997) have an angular resolution of 23'' and a spectral resolution of 2.6 km s⁻¹, while the JCMT CO J=3-2 data have an angular resolution of 14.5'' and a spectral resolution of 0.43 km s⁻¹. We produced three additional data cubes for each galaxy: one binned by 6 channels in velocity, one convolved to achieve a gaussian beam of 23'', and one that was both convolved and binned. From these cubes we made moment 2 maps using the method described in § 2 but using a signal-to-noise cutoff for the mask of 3.5 sigma so as to include only regions with relatively high signal to noise. The average velocity dispersion measured in each map is given in Table A1. These results clearly show that data with poorer spectral or spatial resolution will give higher values for the velocity dispersion than data with better spectral or spatial resolution. The data also suggest that *spatial* resolution may be a more important factor in increasing the measured velocity dispersion than spectral resolution, as long as the spectral resolution is sufficient to resolve the lines. Interestingly, our average velocity dispersions for these two galaxies are only slightly smaller than those measured by Combes & Becquaert (1997) when our data are smoothed spatially and spectrally to match the IRAM data.

We next investigated the effect of the choice of the signal-to-noise cutoff for the masks used in creating the moment map. For this analysis, we used the data cubes that had been smoothed spatially to match the data from Combes & Becquaert (1997) to give better signal-to-noise in our maps, but which had no spectral smoothing applied. The results are given in Table A2. It is clear that the measured velocity dispersion decreases systematically as higher signal-to-noise cutoffs are used in the mask.

Finally, we performed gaussian fits to selected spectra

Table A3. Comparison of velocity dispersion from gaussian fits and second moment maps for selected positions in NGC 3938

Position ^a (" , ")	Gaussian fit (km s ⁻¹)	Moment 2 map ^b (km s ⁻¹)
(0,44)	9.4 ± 2.9	7.8
(0,22)	14.0 ± 2.3	19.3
(0,0)	23.0 ± 4.4	19.3
(0,-22)	8.7 ± 1.3	8.4
(0,-44)	15.0 ± 3.2	8.2

^a All values measured for the CO J=3-2 line. The spectra have been to a 23'' beam and binned to 2.6 km s⁻¹ resolution. (0,0) correspond (11:52:49.6,44:07:17.7 J2000).

^b Measured from maps made using a 2.5 σ cutoff.

from the data cube of NGC 3938 that had been convolved to 23'' and binned to 2.6 km s⁻¹ resolution (Figure A1 and Table A3). To mimic approximately the selection of spectra shown in Combes & Bequaert (1997), we selected the spectrum with the highest velocity dispersion in a map made with a 3.5 σ cutoff, and then stepped away from this spectrum in steps of 3 pixels (21.8'') in the north and south directions. We obtain similar values for the velocity dispersions from fits to the unbinned spectra; binned spectra are shown in Figure A1 for clarity. Although there is considerable scatter in the velocity dispersions for individual spectra, the average value derived from gaussian fits is 1.2 times larger (the standard deviation 0.4) than the value derived from the moment 2 map.

On the basis of this analysis, we opted to use a signal-to-noise cutoff of 2.5 σ on our original data cubes, as this choice seemed to give good agreement with the results from Combes & Bequaert (1997) when both data sets were matched in angular and frequency resolution.

APPENDIX B: THE POSSIBLE EFFECT OF ANISOTROPIES IN THE VELOCITY DISPERSION

There is no statistically significant correlation of velocity dispersion in the molecular gas with inclination in our data (Figure B1). The average observed velocity dispersion is 5.3 km s⁻¹ for the 4 galaxies with inclinations < 25° and 8.1 km s⁻¹ for the 8 galaxies with inclinations > 25° and these values agree within 2 sigma. We have also checked for any correlation of the velocity dispersion normalized by each of the star formation rate and D_{25} with inclination and again find no correlation.

For an inclined galaxy, the observed velocity dispersion is a combination of the in-plane (σ_r, σ_θ) and vertical velocity (σ_z) dispersions. We will assume that $\sigma_r = \sigma_\theta$ and will refer to the in-plane component of the velocity dispersion as σ_r from here on for simplicity. Thus, for a galaxy with inclination i , the observed velocity dispersion is $\sigma_{obs} = \sqrt{\sigma_z^2 \cos^2 i + \sigma_r^2 \sin^2 i}$. If the radial and vertical velocity dispersions of the molecular gas were isotropic, we would not expect any trend of velocity dispersion with inclination. If, however, the velocity ellipsoid of the giant molecular clouds (which contain most of the mass of the molec-

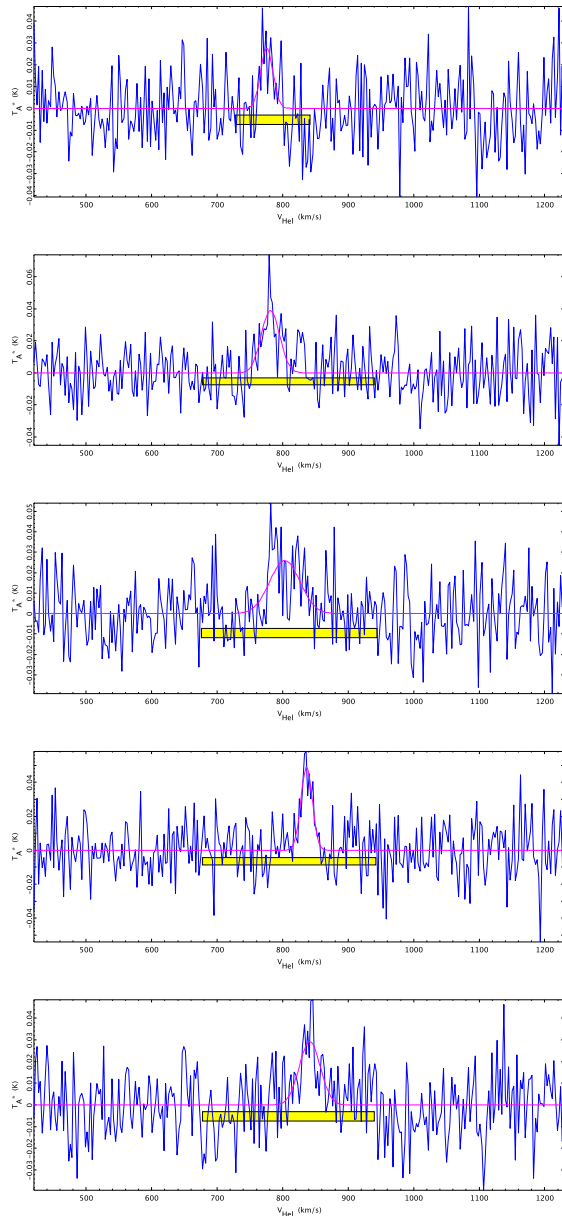


Figure A1. Observed CO $J=3-2$ emission at five positions in NGC 3938. The spectra have been convolved to a 23'' beam and binned to 2.6 km s⁻¹ resolution. Spectra are spaced by 22'' along the declination axis ordered from north (top) to south (bottom) and the central spectrum corresponds to (11:52:49.6,44:07:17.7). Gaussian fits to each spectrum are overlaid; the bar indicates the region used to obtain the fit.

ular ISM) is anisotropic, with $\sigma_r > \sigma_z$, then the observed velocity dispersion would tend to increase with increasing inclination.

Unfortunately, there is no direct information on the shape of the velocity ellipsoid for giant molecular clouds. In theoretical models, the cloud velocity dispersion has been attributed to cloud-cloud scattering (Gammie, Ostriker & Jog 1991) as well as to the driving effects of spiral structure (Thomasson et al. 1991). Since both these models were two-dimensional, they can give us no guidance on the relative strength of the vertical and in-plane velocity dispersions.

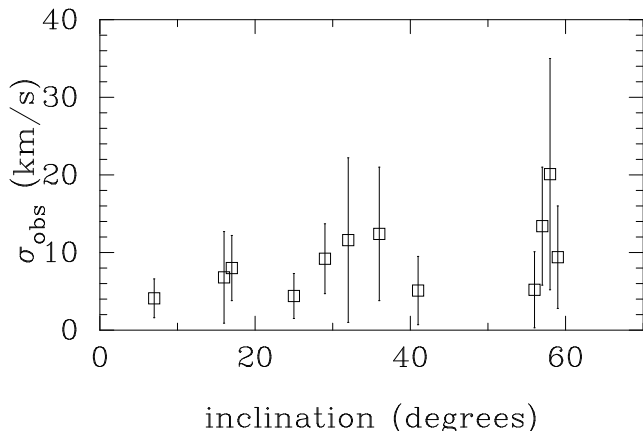


Figure B1. Observed CO $J=3-2$ velocity dispersion as a function of galaxy inclination angle. Error bars show the standard deviation of the observed values within an individual galaxy.

In contrast, there have been a number of studies of the stellar velocity ellipsoid (Delhaye 1965; Dehnen & Binney 1998; Elias et al. 2006). If the velocity ellipsoid of any stars can give us a clue to that of GMCs, it will be the youngest O and B type stars, which may be sufficiently young to still trace the motions of their parent clouds. The smallest values for the velocity ellipsoid can be found in Delhaye (1965), who measured a relative velocity dispersion $\sigma_z/\sigma_r = 0.75$ for 35 O-B5 supergiants. Dehnen & Binney (1998) measure a significantly smaller value of $\sigma_z/\sigma_r = 0.38^{+0.5}_{-0.10}$ for 500 main sequence stars with $-0.24 < B - V < 0.14$. However, this colour range extends well into the A star range where main sequence lifetimes are larger than 100 Myr. Since this velocity dispersion ratio is well known to decrease with the age of the stellar population (Delhaye 1965; Dehnen & Binney 1998), this value may not be an appropriate one to adopt for GMCs. In a recent study of OB stars using Hipparcos data, Elias et al. (2006) obtained a value of $\sigma_z/\sigma_r = 0.64 \pm 0.06$ for 800 stars with spectral types O-B6 within 1 kpc of the Sun. Dividing the sample into stars in the Gould's Belt and the Local Galactic Disk results in values of $\sigma_z/\sigma_r = 0.72 \pm 0.08$ and $\sigma_z/\sigma_r = 0.57 \pm 0.09$, respectively.

Gammie, Ostriker & Jog (1991) caution that a critical difference between star-cloud and cloud-cloud scattering, namely the relative sizes of the epicyclic amplitude and the cloud tidal radius, prevents direct application of stellar results to molecular clouds. However, this model ignores the possible effect of spiral arms, which could conceivably introduce an anisotropy into the cloud motions. In estimating the possible correction to our observed velocity dispersions for the effects of anisotropy in the velocity ellipsoid, we adopt a conservative value of $\sigma_z/\sigma_r = 0.6$, which is the 1σ upper limit obtained by Elias et al. (2006) for their entire sample. With this value, corrections for the velocity ellipsoid only exceed 10% for inclinations greater than 27° .